135 (2022) 212749

Contents lists available at ScienceDirect

Biomaterials Advances

journal homepage: www.journals.elsevier.com/materials-science-and-engineering-c

Novel microgel culture system as semi-solid three-dimensional *in vitro* model for the study of multiple myeloma proliferation and drug resistance

Sandra Clara-Trujillo [a,b,*], Laia Tolosa [b,c], Lourdes Cordón [d,e], Amparo Sempere [d,f], Gloria Gallego Ferrer [a,b], José Luis Gómez Ribelles [a,b]

[a] Centre for Biomaterials and Tissue Engineering (CBIT), Universitat Politècnica de València, Valencia 46022, Spain
[b] Biomedical Research Networking Center on Bioengineering, Biomaterials and Nanomedicine (CIBER-BBN), Valencia 46022, Spain
[c] Experimental Hepatology Unit, Health Research Institute La Fe (IIS La Fe), Valencia 46026, Spain
[d] Centro de Investigación Biomédica en Red de Cáncer (CIBERONC), Instituto Carlos III, Madrid, Spain
[e] Hematology Research Group, Instituto de Investigación Sanitaria La Fe, Valencia, Spain
[f] Hematology Department, Hospital Universitario y Politécnico La Fe, Valencia, Spain

ARTICLE INFO

Keywords:
Multiple myeloma
Microgels
Microspheres
Emulsion polymerization
Drug resistance
Acrylic acid

ABSTRACT

Multiple myeloma (MM) is a hematological malignancy in which the patient's drug resistance is one of the main clinical problems. As 2D cultures do not recapitulate the cellular microenvironment, which has a key role in drug resistance, there is an urgent need for better biomimetic models. Here, a novel 3D platform is used to model MM. The semi-solid culture consists of a dynamic suspension of microspheres and MM cells, termed as microgel. Microspheres are synthesized with acrylic polymers of different sizes, compositions, and functionalities (fibronectin or hyaluronic acid). Optimal conditions for the platform in terms of agitation speed and microsphere size have been determined. With these parameters the system allows good proliferation of the MM cell lines RPMI8226, U226, and MM1.S. Interestingly, when used for drug resistance studies, culture of the three MM cell lines in microgels showed close agreement in revealing the role of acrylic acid in resistance to anti-MM drugs such as dexamethasone and bortezomib. This work presents a unique platform for the *in vitro* modeling of non-solid tumors since it allows keeping non-adherent cells in suspension conditions but in a 3D context that can be easily tuned with different functionalizations.

1. Introduction

Multiple myeloma (MM) is a hematological malignancy characterized by the accumulation of monoclonal plasma cells (PCs) in the bone marrow (BM). MM accounts for 1% of all cancers and 10% of all hematological malignancies [1–4]. Despite advances in the treatment most patients will experience drug resistance (DR) and become refractory to therapies [5]. Better understanding of DR mechanisms in MM is critical to improve novel therapeutic strategies for refractory and relapsed patients.

In MM, DR development presents a complex landscape, due to the genetic heterogeneity of this disease and the complexity of the BM niche [1]. The BM microenvironment (BMME) includes a rich cellular compartment formed by hematopoietic cells (myeloid cells, T and B lymphocytes, and natural killers' cells) and non-hematopoietic cells (fibroblasts, osteoblasts, osteoclasts, endothelial cells, endothelial progenitor cells, pericytes, mesenchymal stem cells or mesenchymal stromal cells among others). It also has a non-cellular compartment which includes soluble factors (cytokines, chemokines and growth factors) and extracellular matrix (ECM) components (collagen, fibronectin, laminin, hyaluronic acid or heparan sulphate) [6]. All of these participate in the formation of specialized niches that play a key role in MM growth, survival and DR [7]. The mechanisms through which ECM components participate in generating DR are diverse: concentration of soluble growth factors or pro-survival cytokines, limitation of chemotherapeutics diffusion or cell adhesion mediated DR (CAM-DR) [8]. CAM-DR is a

Abbreviations: AA, acrylic acid; BM, bone marrow; BMME, bone marrow microenvironment; BTZ, bortezomib; CAM-DR, cell adhesion mediated drug resistance; DEX, dexamethasone; DR, drug resistance; EA, ethyl acrylate; ECM, extracellular matrix; EDGMA, ethylene glycol dimethacrylate; EMA, ethyl methacrylate; FN, fibronectin; HA, hyaluronic acid; MM, multiple myeloma; PCs, plasma cells.

* Corresponding author at: Centre for Biomaterials and Tissue Engineering (CBIT), Universitat Politècnica de València, Valencia 46022, Spain.
E-mail address: sanclatr@doctor.upv.es (S. Clara-Trujillo).

https://doi.org/10.1016/j.bioadv.2022.212749
Received 25 January 2022; Received in revised form 28 February 2022; Accepted 4 March 2022
Available online 17 March 2022

mechanism whereby MM cells escape the cytotoxic effects of anti-cancer therapy *via* adhesive interactions with BM stromal cells and/or ECM components [9–14]. This intricate network of interactions between MM cells and the BMME triggers the up-regulation of many signaling pathways resulting in MM cell proliferation and survival. CAM-DR has been described in common MM treatments such as doxorubicin, melphalan, vincristine or dexamethasone (DEX) in MM cell lines and patients' primary MM cells [14–18]. However, despite all the advances in understanding the role of BMME in the generation of DR in MM, discrepancies are still a problem between *in vitro* efficacy and clinical outcomes of the treatments, as conventional 2D cultures do not recapitulate BMME and its role in DR generation. The lack of the cellular and non-cellular BMME components is one of the limitations of conventional cultures, which hinders validating its results in clinical practice [19]. Including tridimensional architecture in the model should also be considered, as discrepancies between 2D and 3D cultures in proliferation and different cell behaviors have been demonstrated for cancer cells [20]. There is thus an urgent need for the development of cell culture models able to address these limitations and to predict the patient-specific drug response.

Previous models were developed using several materials: synthetic polymers such as acrylic polymers [21] or natural constituents of the ECM (collagen [22], fibrinogen [23], hyaluronic acid [24], PuraMatrix [25]) or even ossified tissues [26]. All proved the convenience of using 3D cultures to recreate MM, and reproduced *in vitro* particular aspects of the disease that were lost in conventional cultures [27]. However, all these studies are based on static architectures in which the substrate has a predefined shape, mainly scaffolds or hydrogels. In this study, we present for the first time a culture platform based on microspheres suspended in a liquid media and coexisting with MM non-adherent cells growing dynamically in suspension, as shown in Fig. 1. This semi-solid culture media, termed a microgel, is inspired by the semi-solid nature of the native ECM. Microgel cultures would create a three-dimensional dynamic context for MM cells and would allow effective and selective presentation of bone marrow ECM molecules to the cells, inasmuch as the microspheres can be modified with different functionalizations. Moreover, cultures are carried out under stirring, thus improving the biomimicry of the system by conferring a dynamic character.

2. Experimental section/methods

2.1. Microsphere's production

Cross-linked copolymeric microspheres were produced with two different compositions (Table 1) following an emulsion polymerization protocol in a sealed 500 mL volumetric flask under magnetic stirring immersed in a jacketed glass beaker connected to a thermostatic water bath. 4% w/v poly(vinyl)alcohol (PVA) (Sigma-Aldrich, USA) (solution in deionized water was used as emulsifier. 100 mL of the dispersion phase were placed into the reactor at 30 °C at 800 rpm. Monomeric mixture (10 g) was washed with 5% w/v sodium hydroxide (NaOH) (Sigma-Aldrich, USA) to remove the inhibitor. For the acrylic acid (AA) (Sigma-Aldrich, USA) -containing microspheres, AA was added after inhibitor removal. The initiator, benzoyl peroxide (BPO) (Fluka, Switzerland), was dissolved within the monomer phase at 0.5% w/w. Reactor temperature was kept at 65 °C for 6 h for polymerization and 1 h at 90 °C for post-polymerization. The microspheres were extensively cleaned with 5% w/v NaCl solution, water, ethanol and acetone. They were then filtered with cell strainers (mesh sizes 60 μm and 70 μm).

Table 1
Microsphere's composition.

Microsphere type	Initiator [g]	Monomer mixture [g]	Monomer mixture formulation		
			Monomer[a]	[g]	% w/w
0% AA	0.05	9.95	EA	5.47	55
			EMA	3.48	35
			EGDMA	0.99	10
			AA	0	0
10% AA	0.05	9.95	EA	4.97	50
			EMA	2.99	30
			EGDMA	0.99	10
			AA	0.99	10

[a] EA (ethyl acrylate) (Sigma-Aldrich, USA), EMA (ethyl methacrylate) (Sigma-Aldrich, USA), EGDMA (ethylene glycol dimethacrylate) (Sigma-Aldrich, USA), and AA (acrylic acid).

2.2. Microsphere's functionalization

Fibronectin (FN) (Sigma-Aldrich, USA) was adsorbed on 0% AA microspheres at 20 μg mL^{-1} in milliQ water for 1 h at RT in an orbital shaker. Bovine serum albumin (BSA) (Sigma-Aldrich, USA) was adsorbed on 10% AA and 0% AA microspheres at 1 mg/mL in milliQ water, overnight at room temperature (RT) in an orbital shaker. After adsorption, the samples were rinsed twice in phosphate buffered saline (PBS). To test BSA adsorption, BSA conjugated with fluorescein-5-isothiocyanate (FITC) (Invitrogen, USA) was used and samples were imaged under an epifluorescence Eclipse 80i microscope (Nikon, Japan) in comparison with non-coated samples. The micro bicinchoninic acid assay (BCA) Protein Assay Kit (Thermo Scientific, USA) was used to quantify the amount of FN adsorbed, following the manufacturer's protocol. Coated and uncoated samples were analyzed on a Victor 3 microplate reader (Perkin Elmer, USA), reading at 550–570 nm.

Hyaluronic acid (HA) (Sigma-Aldrich, USA) molecular weight was

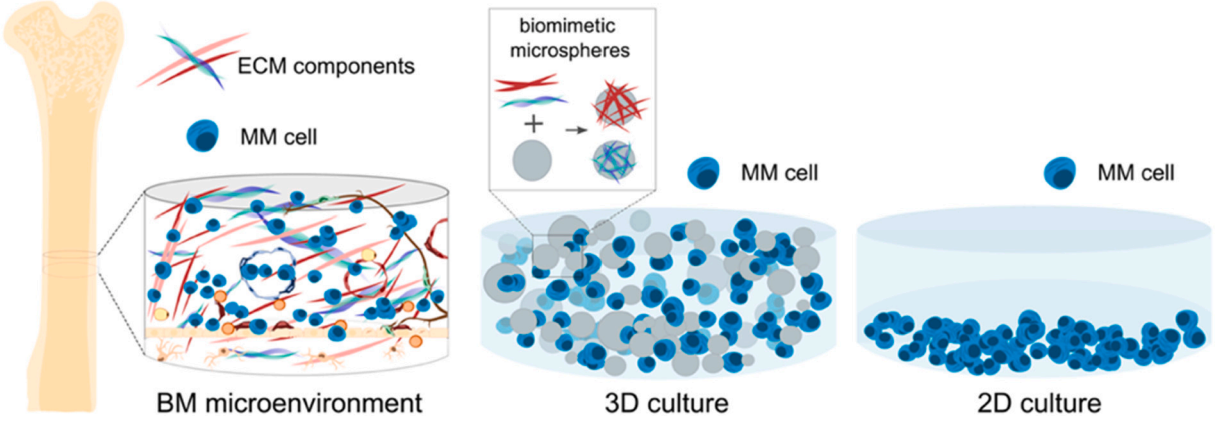

Fig. 1. Scheme of the *in vivo* bone marrow microenvironment of MM cells and the cell culture system developed for the microgel compared with the conventional 2D culture.

reduced from 106 MDa to 320,000 Da by means of acidic degradation [28]. The resulting low molecular weight HA was used for microsphere functionalization using a two-step 1-ethyl-3-(3-dimethylaminopropyl) carbodiimide hydrochloride (EDC) (Sigma-Aldrich, USA)/N-hydroxy sulfo-succinimide (sulfo-NHS) (Sigma-Aldrich, USA) coupling. 10% AA microspheres were washed with activation buffer (0.1 M 2-morpholinoethanesulfonic acid (MES) (Sigma-Aldrich, USA), 0.5 M NaCl, pH 6). EDC (2 mM) and sulfo-NHS (5 mM) prepared in an activation buffer were then added to the microsphere pellets at 10 (EDC): 25 (sulfo-NHS): 1 (−COOH) groups on the microsphere surface. Reaction components were mixed and kept in an orbital shaker for 2 h at RT. Two washes were done with PBS pH 7.4. Activated −COOH groups were made to react with a molecular bridge, a di-amine terminated poly(ethylene glycol) (PEG-diNH$_2$) (Sigma-Aldrich, USA) by incubation of the microspheres pellets in 2 mM PEG-diNH$_2$ solution prepared in PBS, 10:1 PEGdiNH$_2$ to −COOH microspheres and kept in an orbital shaker overnight at RT. Two washes were performed with PBS pH 7.4. HA dissolved at 5% w/v in PBS. 100 equivalents of EDC and 40 of sulfo-NHS were added to the HA. The resulting solution was added to microsphere pellets in a proportion of 1 equivalent of HA to 1 equivalent of −COOH microspheres. Mixture was kept overnight (ON) at RT in an orbital shaker. Finally, 2 cleanings in PBS were performed. To assess −COOH presence on the microsphere surface after HA grafting, the indirect toluidine blue O (TBO) assay was performed [29]. For −COOH blocking, 10%AA microspheres were activated under the same conditions and subsequently incubated with 1 M ethanolamine (Sigma-Aldrich, USA), pH 9 for 1 h at 4 °C.

2.3. Microsphere characterization

The surface morphology of the microspheres was observed under a field emission scanning electron microscope (FESEM) (Ultra 55, Zeiss Auriga Compact, Germany). Images were taken at an accelerating voltage of 1 kV. The microspheres were coated with platinum following a standard sputtering protocol for 90 s (JF1100, JEOL, Japan). Their diameter was assessed from white field-inverted microscope images. At least 350 microspheres of each type were measured by ImageJ software (National Institutes of Health, USA).

Thermogravimetric measurements (TGA) of dry and wet samples of 0% and 10%AA microspheres were made by an SDT-Q600 system (TA Instruments, Great Britain). Dry samples were vacuum dried. Wet samples were immersed in liquid water and left to equilibrate for 48 h. TGA tests were carried out in alumina pans in which samples of about 5–10 mg were heated from 30 °C to 800 °C at a rate of 10 °C min^{-1} in a nitrogen atmosphere of 20 mL min^{-1} flow. The equilibrium water content (EWC) was calculated from the experimental TGA measurements of the wet samples, taking into account that at 100 °C the water they initially contained had evaporated and that the weight of the samples at the beginning of the TGA experiments (initial wet weight) were normalized to 100% (Eq. (1)):

Calculation of EWC (wt%) from TGA experiments

$$\mathrm{EWC}\ (\mathrm{wt.\%}) = \frac{m_{H_2O}}{m_{dry}} \times 100 = \frac{\text{initial wet weight } 100\% - \text{dry weight\% at } 100^{\circ}\mathrm{C}}{\text{dry weight\% at } 100^{\circ}\mathrm{C}} \times 100 \quad (1)$$

where m_{H2O} and m_{dry} are the mass of water the microspheres absorb at equilibrium and the mass of the dry polymeric microspheres, respectively.

Acrylic acid inclusion in the microspheres and different functionalizations were assessed by X-ray photoelectron spectroscopy (XPS) on an XPS Spectrometer AXIS Supra (Kratos Analytical, Japan), which uses a monochromatic Al Kα X-ray source (1486.6 eV) covering an analyzing area of 700 × 300 μm (120 W power). Survey spectra were collected using a pass energy of 160 eV and a step size of 1 eV. High-resolution regions were collected at a pass energy of 20 eV and a step size of 0.1 eV. Data were processed on CasaXPS (Casa Software, United Kingdom) software.

2.4. Microsphere sterilization

Microspheres were sterilized with 3 cleanings in 70% ethanol of 10 min each at RT in an orbital shaker. Then 3 washes in sterile Dulbecco's phosphate buffered saline (DPBS) were performed.

2.5. Cell lines

The multiple myeloma (MM) cell lines RPMI8226, U226-B1 and MM.1S were purchased from the American Type Culture Collection (ATCC, Rockville, MD). MM cell lines were cultured in RPMI1640 media (Gibco, USA) supplemented with 10% fetal bovine serum (FBS) (Gibco, USA), 2 mM L-glutamine (Lonza, Switzerland) and 100 μg mL^{-1} penicillin, and 100 μg mL^{-1} streptomycin (Life Technologies, USA). All cells were cultured at 37 °C and in 5% CO_2 in a Galaxy S incubator (Eppendorf New Brunswick, Germany).

2.6. Development of 3D microgel cultures

For microgel cultures, 100,000 cells were seeded in 500 μL of 7% v/v microsphere's suspension in complete cell culture media in non-treated p24 cell culture microplates. For conventional suspension cultures, each well was formed by 100,000 cells and 500 μL of media. Cell cultures were carried out under dynamic conditions in a PMS-1000i microplate shaker (GrantBio, UK). Each 24 h 50% volume of media culture was renewed.

2.7. Cell proliferation

Cell proliferation was determined by colorimetric 3-(4,5-dimethylthiazol-2-yl)-5-(3-carboxymethoxyphenyl)-2-(4-sulfophenyl)-2H-tetrazolium) (MTS) (Promega, USA) assay following manufacturer's instructions. Supernatant was pipetted onto a 96-well plate and read at 490 nm (Victor 3 microplate reader, Perkin Elmer, USA). After blank subtraction, absorbance data was converted to cell number by using a calibration curve for each cell line. Results are given as % of MM proliferation from Day 0, considering the initial cell number as 100%. MM proliferation (% of Day 0) was calculated using Eq. (2):

Calculation of MM proliferation (% of Day 0)

$$\text{MM proliferation (\%of Day 0)} = \left(\text{cell number at 72 h} \times \text{cell number at Day 0}^{-1}\right) \times 100 \quad (2)$$

where cell number at 72 h was obtained from MTS results as described and 100,000 cells (seeding density) was considered as cell number at Day 0.

2.8. Ki67 expression

After 72 h of culture, cell culture wells were pre-fixed by adding 500 μL of 4% paraformaldehyde, 5 min at RT. 2 cleanings with PBS were performed and cells were fixed for 20 min at RT with 2% paraformaldehyde. Samples were permeabilized and blocked in 10% (v/v) FBS in DPBS/0.1% (v/v) Triton-X100 (Sigma-Aldrich, USA)for 1 h at RT and incubated with primary polyclonal antibody against Ki67 (Abcam, UK, 1:25) in blocking buffer (10% FBS in DPBS/0.1% Triton-X100) overnight at 4 °C. The samples were then rinsed twice in DPBS/0.1% Triton X-100 and incubated with the secondary antibody (Alexa Fluor 555, Invitrogen, USA, 1:500) and BODIPY FL phalloidin (Invitrogen, USA, 1:500) prepared in blocking buffer RT for 1 h. Finally, they were washed twice in DPBS/0.1% Triton X-100 before mounting with Vectashield containing DAPI (Vector Laboratories, USA) and observed under an epifluorescence microscope (Nikon Eclipse 80i) at 60×. Image analysis was by Cell Profiller [30] and MATLAB (R2018b, MathWorks Inc., Natick, MA, USA). Cell segmentation was performed by Cell Profiller. Briefly, DAPI images were thresholded (by an Otsu adaptative two-classes thresholding method) and used for nuclear segmentation. The intensity of protein staining (sum of intensities of all pixels) and the region of interest area (total number of pixels) was quantified by the obtained nuclear masks in the Ki67 images using an inhouse software tool developed in MATLAB. Mean fluorescence intensity was obtained for each cell following Eq. (3).

Calculation of the total number of cells for Live/Dead staining

$$\text{Mean fluorescence intensity (a.u.)} \times \text{cell}^{-1} = \text{sum of all pixels intensities} \times \text{total pixels}^{-1} \quad (3)$$

Data is expressed as mean fluorescence intensity per cell and at least 18 cells per condition from 6 different pictures of 3 different samples were analyzed for each condition.

2.9. Drug resistance in microgel cultures

The different MM cell lines were cultured in the different microgels of interest and in suspension for 72 h in presence of Dexamethasone 1 μM (DEX) (Fortecortin, Merck KGaA, Germany), Bortezomib 4 nM (BTZ) (STADA, Germany) or absence of drugs (non-treated).

2.10. Cell viability

Live/Dead assay (Thermo Fisher, USA) was used following the manufacturer's instructions. Then, samples were washed twice with DPBS, extended on a cover glass, and imaged at 10× using an epifluorescence microscope (Nikon Eclipse 80i). Six different fields of each sample were analyzed on ImageJ 1.51v (National Institutes of Health, USA) using the Find Maxima process tool. The total number of cells was calculated by Eq. (4) and the percentage of cell viability was calculated as per Eq. (5).

Calculation of the total number of cells for Live/Dead staining

$$\text{N total} = \text{live cells} + \text{dead cells} \quad (4)$$

where *live cells* are the total number of cells quantified using the calcein channel. Dead cells are the total number of cells quantified in the ethidium homodimer-1 stain.

Calculation of Live Cells (%) for Live/Dead

$$\text{Live Cells (\%)} = \left(\text{live cells} \times \text{N total}^{-1}\right) \times 100 \quad (5)$$

2.11. Statistical analysis and reproducibility

Cell culture experiments were performed in triplicates and repeated at least twice individually ($n \geq 6$). Results are given as mean ± standard deviation (SD). For statistical analysis, the data were analyzed for normality using the Shapiro-Wilk normality test with an alpha of 0.05. For comparisons of three or more groups when the normality test was passed an ordinary one-way ANOVA test and Tukey's post-hoc test ($p = 0.05$) were used to perform multiple comparisons between the column means. When the normality test was not passed, a non-parametric Kruskal-Wallis test was used with a post-hoc Dunn analysis ($p = 0.05$) to perform multiple comparisons between the column means. GraphPad Prism 9 software (GraphPad Software, USA) was used for statistical analysis. Differences among groups are stated as $p \leq 0.05$ (*), $p \leq 0.01$ (**), $p \leq 0.001$ (***), $p \leq 0.0001$ (****). All graphs were created with the ggplot2 [31] package in R language, using the R studio version 1.3.1093 (R Development Core Team, Vienna, Austria).

3. Results and discussion

3.1. Biostable microspheres with different sizes, chemistries and functionalizations

3.1.1. Obtaining the microspheres with 0% and 10% of acrylic acid

Polymeric biostable microspheres have been obtained with two different compositions. The copolymers consisted of ethyl acrylate (EA), ethyl methacrylate (EMA) and ethylene glycol dimethacrylate (EGDMA); the two types differentiate in the presence (10%) or absence (0%) of acrylic acid (AA). Polymeric composition was chosen based on the specific properties of each monomer. Poly(EA) (better known as PEA) induces fibronectin (FN) fibrillogenesis in the absence of cellular activity [32,33], EMA was incorporated to increase the glass transition temperature and make the

Table 2
Descriptive statistics from the diameter distributions of the different fractions obtained after sieving the 0% AA and 10% AA microspheres.

Polymer composition	Sieved fraction	Mean diameter (μm) ± Standard deviation	Minimum diameter (μm)	Maximum diameter (μm)
0% AA	<60 μm	15 ± 11	2	66
10% AA	<60 μm	31 ± 19	4	102
10% AA	>70 μm	86 ± 19	22	220

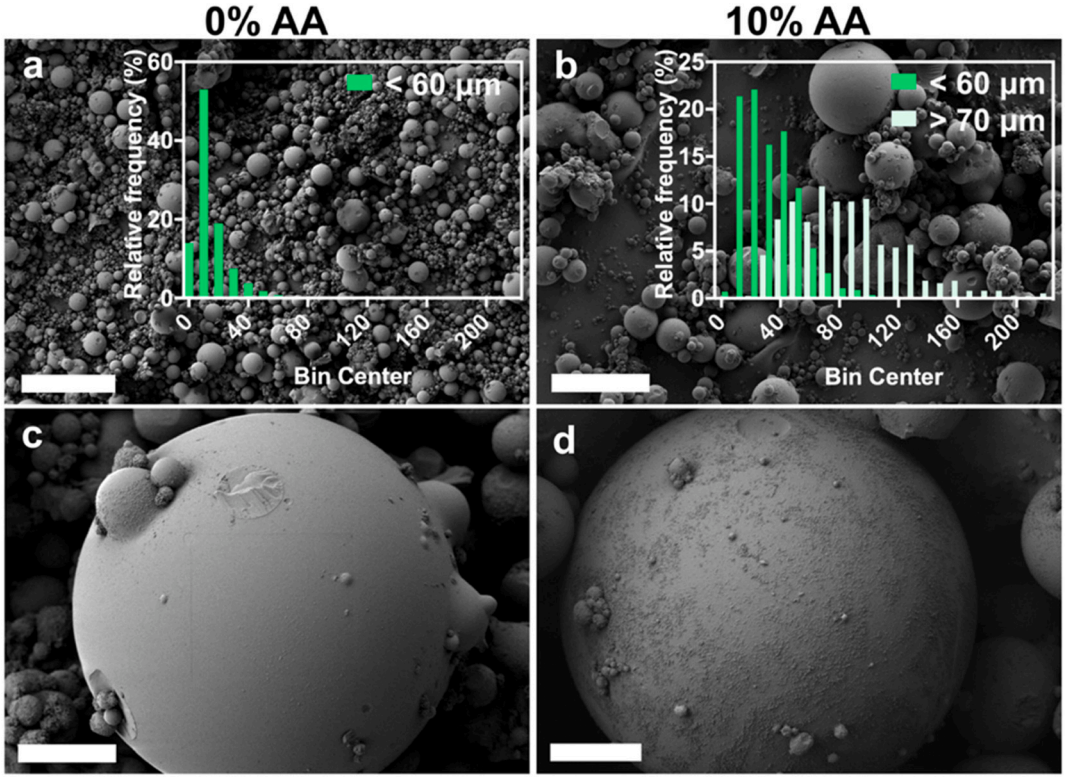

Fig. 2. Acrylates-based biostable microspheres with different sizes and compositions. FESEM (field emission scanning electron microscope) images of non-sieved 0% (a) and 10% (b) AA (acrylic acid) microspheres with the diameter distributions of the different size fractions separated after sieving (inserted histograms, bin size: 10 µm, at least 350 microspheres of each type were measured using ImageJ software (National Institutes of Health, USA), results are plotted in relative frequency (%)). Scale bar: 100 µm. c, d) Detail of microspheres topography. Scale bar: 10 µm.

microspheres easier to handle [34], and EGDMA as crosslinker to make them compatible with ethanol-based sterilization methods. AA provides carboxyl functional groups, which allow different molecular grafts based on amide bonds [34,35]. As we intended to study the effect of microsphere size on cell proliferation, the microspheres were sieved and separated into <60 µm diameter and >70 µm diameter fractions. The descriptive statistics of the diameter distribution of the three different microsphere fractions obtained are shown in Table 2.

The <60 µm fraction presents diameter distributions similar to the cell size of MM cells (approximately 10 µm diameter) (Fig. 2 a, b). Field emission scanning electron microscope (FESEM) images confirmed a regular spherical morphology and showed that 10% of the AA microspheres have a rougher topography than 0% AA (Fig. 2 c, d), with satellite nanospheres on the surface. Polymerization takes place in microdroplets of the organic phase containing EA, EMA, EDGMA and the initiator, immersed in an agitated aqueous phase, and the AA is soluble both in the organic and aqueous phases. We hypothesized that, once polymerization has started inside the organic microdroplets, nanodroplets of AA migrate from the aqueous to the organic phase and polymerize preferentially on the microsphere surface giving rise to this topography [36]. This phenomenon could also justify the larger diameters obtained by the 10% AA microspheres.

As seen in Fig. 3 a, the 0% AA have a statistically significant higher signal of Toluidine Blue O (TBO) stain, confirming the presence of AA on their surface. A thermogravimetric analysis (TGA) of vacuum dried and wet samples was also performed (after equilibration in liquid water for 48 h) of 0% and 10% AA microspheres (Fig. 3 b). The weight loss of up to 100 °C can determine the equilibrium water content (EWC) of the microspheres. Water sorption is 0.58 g of water per gram of polymer, *i.e.*, EWC = 58 wt% measured on a dry basis in the 10% AA sample due to the presence of the hydrophilic carboxylic groups of the monomeric units of poly(AA), which act as sorption sites for water molecules. The equilibrium water sorption of 0%AA sample is much smaller, in the order of EWC = 8.3 wt%, typical of hydrophobic acrylates that do not contain hydrophilic groups [37,38]. An X-ray photoelectron spectroscopy (XPS) analysis was carried out to further explore AA incorporation on the 10% microspheres. Elemental composition extracted from the survey spectra of 0% and 10% AA samples (Fig. 3 c) was used to calculate the experimental O/C ratio that was plotted against the theoretical O/C ratio (calculated from the molecular formula of each monomer and the polymeric composition), (Fig. 3 d). The experimental O/C ratios showed lower values than theoretical values for both types of microsphere. Due to the higher proportion of O atoms in the acrylic acid monomer, the difference between the 10% AA and 0% AA ratio confirmed AA incorporation onto the surface of the 10% microspheres. This difference was greater in the experimental O/C ratios than the theoretical, which can be attributed to the preferential polymerization of AA on the microsphere surface than in the bulk [36], reinforcing the hypothesis made when studying the microsphere topography and diameter distributions. The scan spectra of C1s and O1s of both types of microsphere are shown in Fig. 3 e. As expected, new peaks were not observed due to the incorporation of the AA, nevertheless the intensity of the (C═O)—O and the C—O peaks in the 10% AA C1s scan was higher than the C1 scan of the 0% AA microspheres. The intensity of the (C═O)—O peak was also higher in the 10% AA O1 scan than the O1 scan of the 0% AA microspheres. These characterizations thus confirmed AA incorporation into the 10% AA microspheres.

3.1.2. FN and HA functionalization of the microspheres

ECM has been established as a key player in the development of MM disease and DR acquisition [7,39,40]. The proteinaceous ECM matrix (mainly composed of fibronectin, laminin and collagens) is the main holder of the BM architecture [41]. The adhesion of MM cells to fibronectin is one of the most frequently studied interactions that generate a

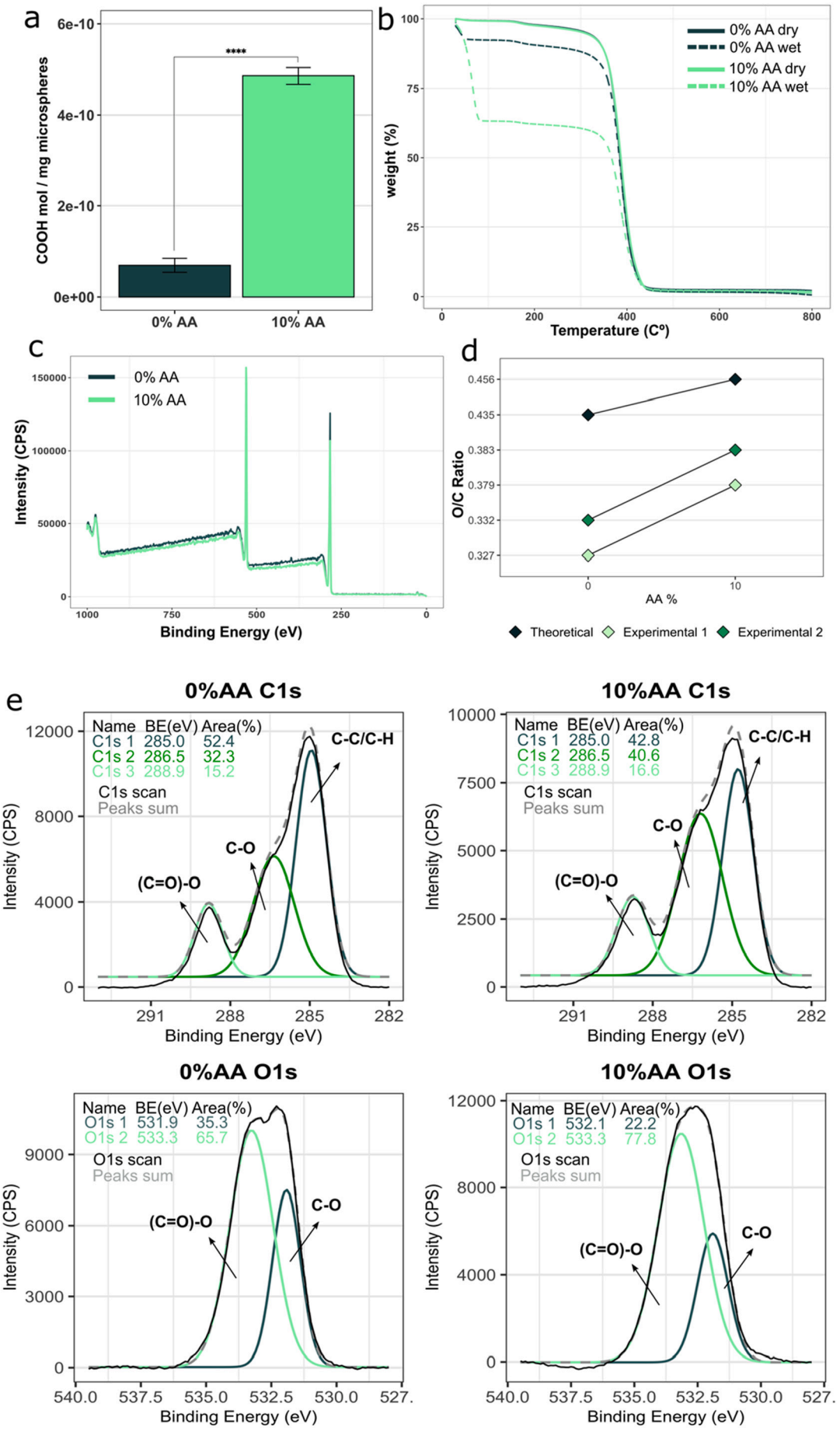

(caption on next page)

Fig. 3. Characterization of acrylic acid (AA) presence on 10% AA microspheres. a) Toluidine Blue O (TBO) colorimetric determination of COOH groups (n = 3, measured in duplicate, comparisons were made using one-way ANOVA with Tukey's test for post-hoc analysis), p value legend: p ≤ 0.0001 (****). b) Thermogravimetric analysis (TGA) of wet (dashed lines) and dry (solid lines) samples of 0% AA and 10% AA microspheres. c) X-ray photoelectron spectroscopy (XPS) survey spectra of 0% AA and 10% AA microspheres. d) Theoretical and experimental O/C ratios calculated from elemental composition of 0% AA and 10% AA microspheres. For experimental ratios, n = 2 XPS survey spectra were analyzed. e) XPS scan spectra of C1s and O1s for 0% and 10% AA microspheres. (For interpretation of the references to color in this figure legend, the reader is referred to the web version of this article.)

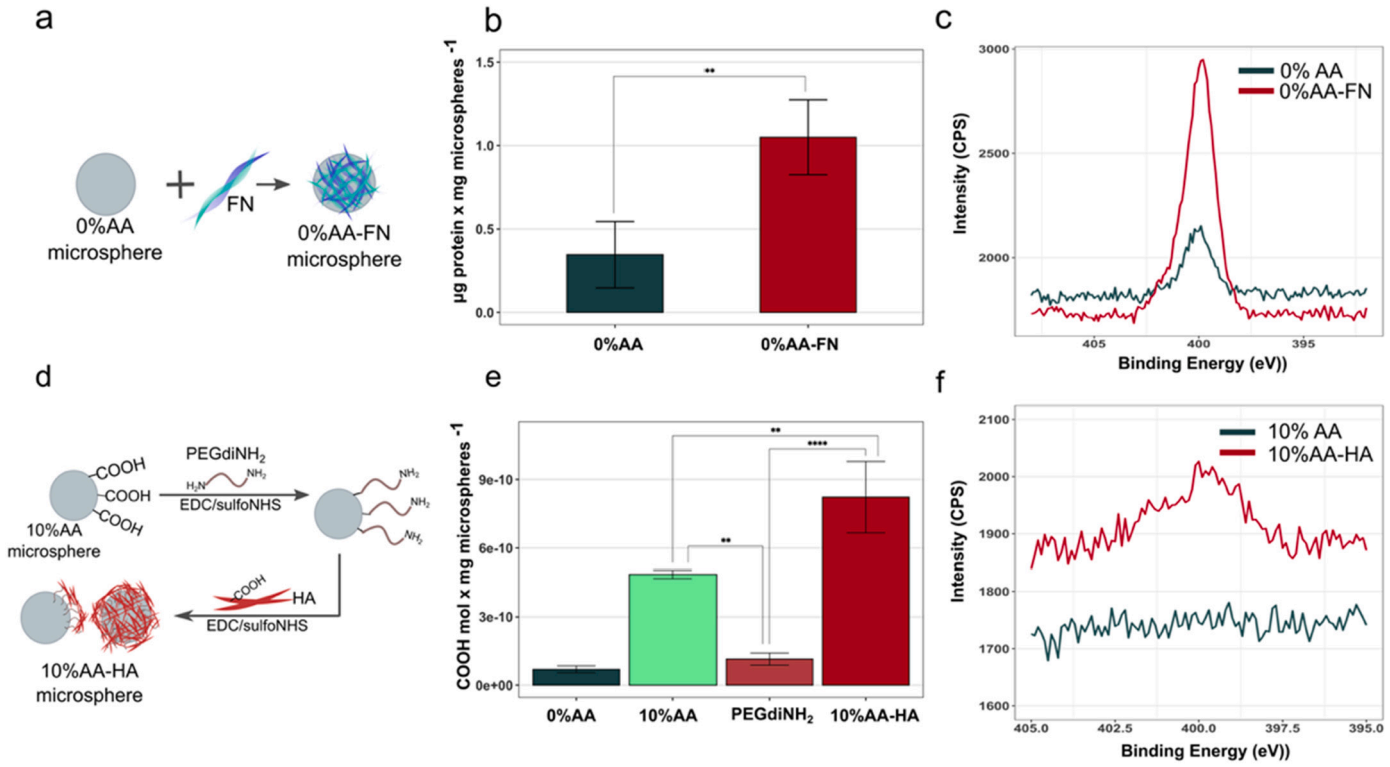

Fig. 4. Characterization of microsphere functionalization. a) Scheme of fibronectin (FN) coating on 0%AA microspheres. b) microBCA assay results for FN coated and non-coated 0%AA microspheres (n = 3, measured in duplicate, comparisons were made using one-way ANOVA with Tukey's test for post-hoc analysis). c) XPS scan spectra of N1s for FN coated and uncoated 0% AA microspheres. d) Scheme of hyaluronic acid (HA) grafting process applied to 10%AA microspheres. e) Toluidine Blue O (TBO) colorimetric determination of COOH groups from 10%AA microspheres at the different stages of the HA grafting process (n = 3, measured in duplicate, comparisons were made using one-way ANOVA with Tukey's test for post-hoc analysis). f) XPS scan spectra of N1s for HA-grafted and ungrafted 10% AA microspheres. p value legend: p ≤ 0.05 (*), p ≤ 0.01 (**), p ≤ 0.001 (***), p ≤ 0.0001 (****). (For interpretation of the references to color in this figure legend, the reader is referred to the web version of this article.)

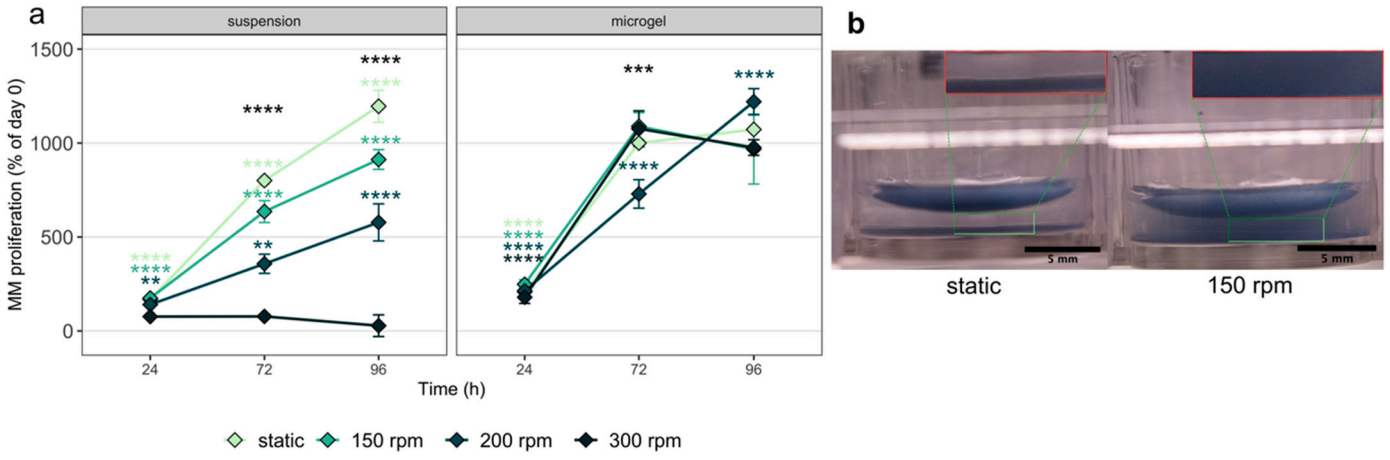

Fig. 5. a) Growth of the RPMI8226 cell line in suspension and microgel cultures at different agitation speeds (static and 150, 200 or 300 rpm). b) Microgel distribution in cell culture wells at 24 h of simulated culture (microspheres were stained in dark blue for visualization) under static and 150 rpm stirring. Comparisons between different time points for each speed and, at each time point between different speeds, were made using one-way ANOVA with Tukey's test for post-hoc analysis. p value legend: p ≤ 0.05 (*), p ≤ 0.01 (**), p ≤ 0.001 (***), p ≤ 0.0001 (****). Statistical differences shown in each stirring speed color refer to differences of this point with the different time points of the same speed. Statistical differences shown in black refer to differences between different stirring speeds at the same time point. (For interpretation of the references to color in this figure legend, the reader is referred to the web version of this article.)

DR phenotype in MM cells and is mediated through integrins α4β1 and α4β5 [9,14,41]. Glycosaminoglycans are incorporated into BM ECM by stromal cells. Hyaluronic acid (HA) is a major component of BM ECM and its adhesive interaction with MM cells, mainly mediated by CD44 and the receptor for hyaluronan-mediated motility (RHAMM) [42], has been related to MM BM homing and the generation of DR [8–10]. The nature of glycosaminoglycans allows them to act as reservoirs of soluble factors from the milieu [8]. Our aim was to study the effect of different ECM components on 3D microgels in the development of DR in MM cell lines. For this purpose we selected FN [7,14], and HA as ECM components [19].

In the case of FN, covalent graft of FN by means of EDC/NHS chemistry is reported to increase probability of blocking key FN active sites, as it involves amino FN groups which are randomly distributed throughout the molecule [43]. Accordingly, FN was adsorbed on the microsphere surface following a conventional coating protocol. 0% AA microspheres were used (Fig. 4 a), as AA has been reported to reduce the efficiency of FN absorption on acrylic copolymers (Supplementary Fig. 1) [44]. The microBCA was used to quantify FN incorporation (Fig. 4 b), and XPS analysis also confirmed the presence of N on the surface of the coated microspheres (Fig. 4 c). HA was incorporated into the microspheres through covalent grafting using 10%AA microspheres (Fig. 4 d). A low molecular weight HA (~320,000 Da) [32] was used and the TBO indirect method to monitor the variation of COOH groups (Fig. 4 e) on the microsphere surface across the sequential steps of the grafting process (Fig. 4 d). The XPS N1s spectra showed the presence of N on the grafted microspheres (Fig. 4 f). Both biomolecules were effectively incorporated onto the microsphere surface by different procedures.

3.2. MM cell proliferation on 3D microgel cultures

3.2.1. 150 rpm stirring maintain 3D microgel cultures in suspension and allow MM cell proliferation

The dynamic physiology of the BM niche is not considered in conventional static cultures [45,46] or 3D cultures with predefined and static architectures [23,24]. This semi-solid platform creates a dynamic context, as cultures are carried out on agitated plates. An initial experiment with the RPMI8226 MM cell line and 10% AA microgel (without functionalization) was conducted to assess the effect of agitation speeds on cell proliferation. Static culture conditions were not chosen, to avoid deposition of the microgel in the bottom of the well, as shown in Fig. 5 b. 150 rpm was chosen as the optimal speed for the subsequent cultures agitation, as it was enough to maintain microgel suspension. After 72 h of culture, the microgel was rated a higher cell proliferation than its suspension counterparts for all the agitation speeds tested (Fig. 5 a). Increasing the agitation speed had a negative impact on cell proliferation of the suspension cultures, a behavior that has been previously reported when culturing different cell lines in agitated bioreactors or spinner flasks [47,48]. Interestingly, this negative effect was overcome by the microgel, which promoted better MM cell growth under stirring.

3.2.2. Microsphere size modulates MM cell proliferation

To determine the effect of microsphere size on MM cell proliferation, <60 μm and >70 μm diameter sizes of the 10% AA microgel without functionalization were cultured with the RPMI8226, U226 and MM1S cell lines. The microgel with microsphere sizes closest to cellular size (<60 μm) had higher cell proliferation after 3 days of culture than those of >70 μm diameter (Fig. 6 a). The >70 μm microgel achieved less

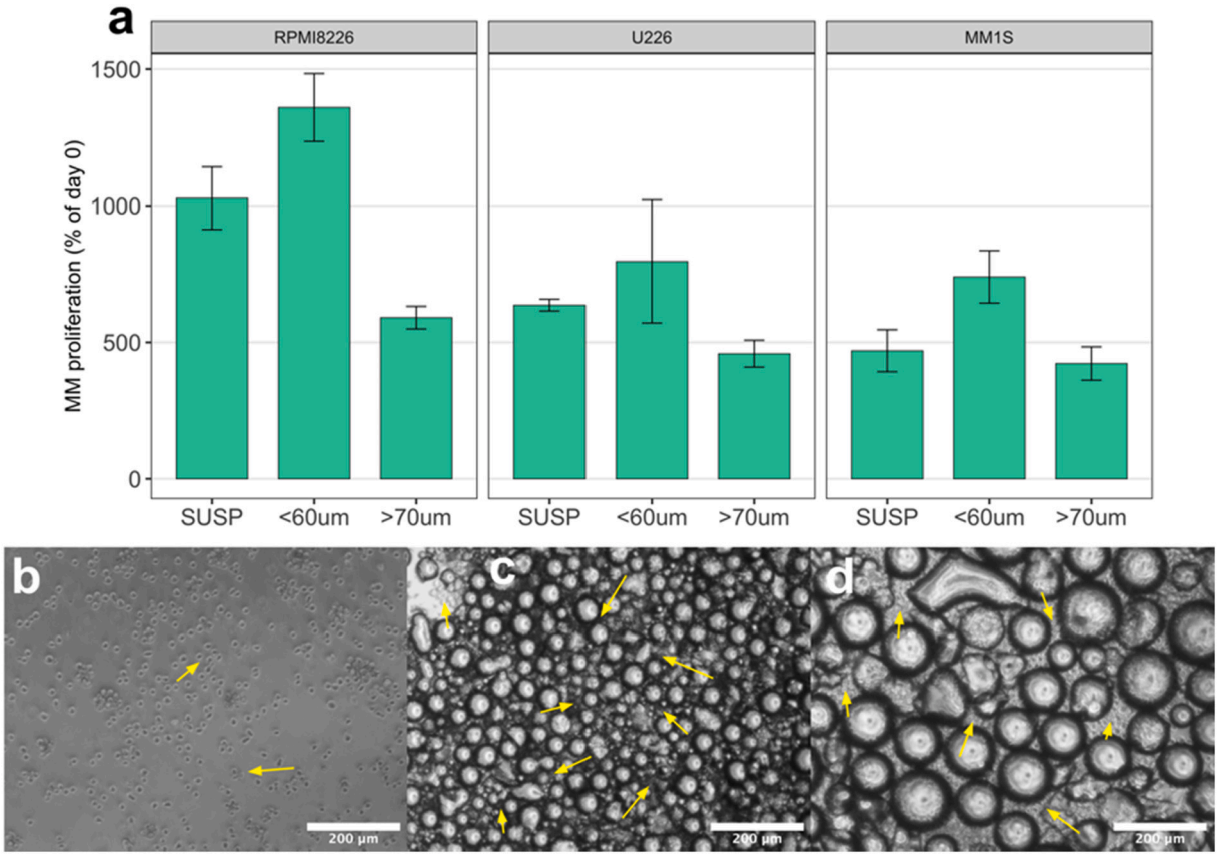

Fig. 6. a) Growth of MM cell lines after 72 h of culture in suspension or in 10% AA microgels with different diameters. b–d) Inverted microscope images at 72 h of RPMI8226 cells cultured in suspension (b), microgel <60 μm diameter (c) and > 70 μm diameter (d). Yellow arrows point to some MM cells. p value legend: $p \leq 0.001$ (***). Scale bar: 200 μm. Comparisons were made using one-way ANOVA with Tukey's test for post-hoc analysis. (For interpretation of the references to color in this figure legend, the reader is referred to the web version of this article.)

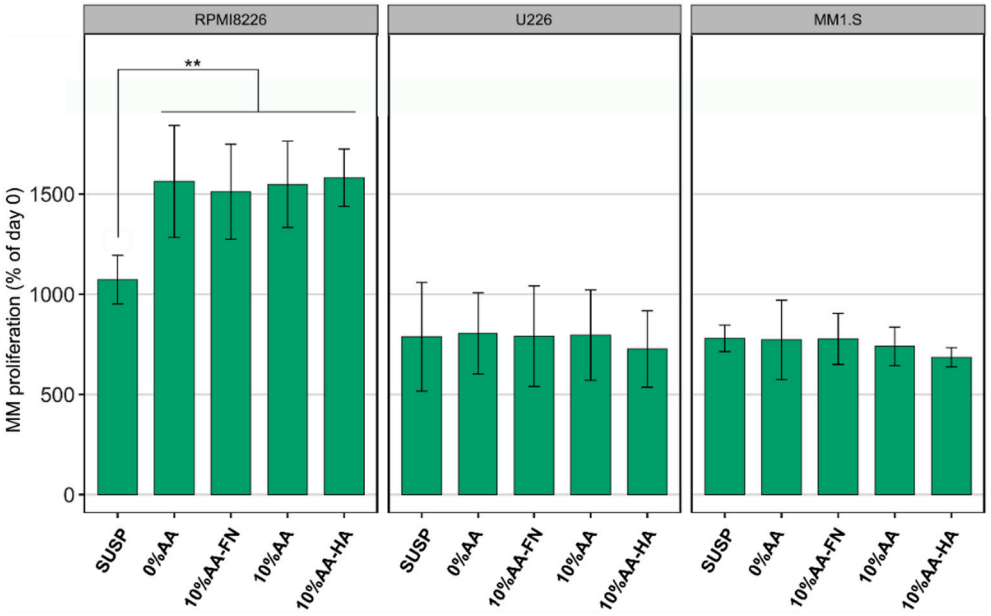

Fig. 7. Growth of the cell lines RPMI8226, U226 and MM1.S after 72 h of culture in suspension or in microgels. Cultures were performed at 150 rpm. SUSP (suspension 2D culture), 0% AA, 0%AA-FN (0% AA coated with fibronectin microgel), 10% AA (10% AA ungrafted microgel), 10%AA-HA (10% AA grafted with hyaluronic acid microgel). p value legend: $p \leq 0.01$ (**). For each cell line, comparisons between microgels were made using one-way ANOVA with Tukey's test for post-hoc analysis.

proliferation than the suspension culture without a microgel and did not distribute homogenously with the cells. Due to its higher weight in the conditions of 150 rpm microspheres it did not stay in suspension and fell to the bottom of the well, causing a cell distribution similar to the culture without a microgel (Fig. 6 b), but with less space for cell growth due to the microspheres (Fig. 6 d). The smallest diameter microgels (Fig. 6 c) achieved a higher specific surface area, meaning increased cell contact with the 3D matrix. Due to their lighter weight, 150 rpm stirring kept the cells and microspheres in suspension and generated a homogeneous 3D distribution (Fig. 6 c). The <60 μm diameter microspheres were thus used for subsequent experiments at an agitation of 150 rpm.

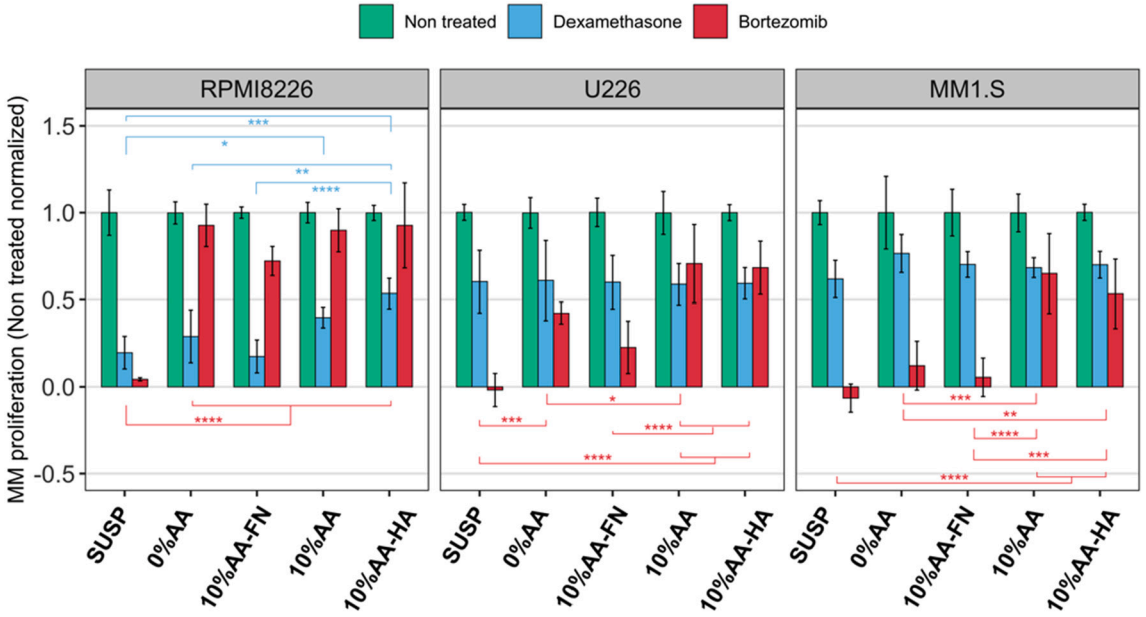

Fig. 8. Proliferation rates of the cell lines RPMI8226, U226 and MM1.S at 72 h of culture growing in suspension or in microgels when treated with dexamethasone 1 μM (blue), bortezomib 4 nM (red) or non-treated conditions (green). Data is expressed as % of MM proliferation with respect to day 0 and, for each condition, normalized by its non-treated counterpart. SUSP (suspension 2D culture), 0% AA (0% AA uncoated microgel), 0%AA-FN (0% AA coated with fibronectin microgel), 10% AA (10% AA ungrafted microgel), 10%AA-HA (10% AA grafted with hyaluronic acid microgel). Statistical differences shown in blue represent differences between DEX treated samples. Statistical differences shown in red represent differences between BTZ treated samples. p value legend: $p \leq 0.05$ (*), $p \leq 0.01$ (**), $p \leq 0.001$ (***), $p \leq 0.0001$ (****). For each cell line, comparisons were made independently for each drug. Comparisons between microgels were made using one-way ANOVA with Tukey's test for post-hoc analysis. (For interpretation of the references to color in this figure legend, the reader is referred to the web version of this article.)

3.2.3. Microgel-based cultures allow proliferation of different MM cell lines

The 10%AA microspheres were thus covalently grafted with hyaluronic acid (10% AA-HA) and those with 0% AA were coated with fibronectin (0% AA-FN). The effect was studied for the functionalized and non-functionalized microgels based on these 2 different polymeric compositions on MM proliferation. To approximate the heterogeneity of the disease, 3 different human multiple myeloma cell lines were used: RPMI8226, U226 and MM1.S (Fig. 7). When cultured on all the different microgels the U226 and MM1.S cell lines showed proliferation rates similar to their suspension cultures, implying that the presence of the microgels does not affect cell proliferation in these cell lines regardless of the composition (0 or 10% AA) or functionalization (FN, HA or none). In the case of the RPMI8226 cell line, all the microgels tested showed higher proliferation rates than those grown in suspension. We attribute this positive effect of the microgels on cell proliferation to the three-dimensionality achieved by the cell-sized microgel, regardless of its composition or functionalization.

The cell and microsphere distribution in the different microgels after 72 h of culture is shown in Supplementary Fig. 2. Although the architecture and original distribution of the well was not strictly preserved (immunofluorescence was performed using a suspension protocol), the cells remained mostly in suspension and did not adhere to the microspheres. This applies to all microspheres with the exception of the microgels coated with FN, in which most of the cells appear forming aggregates between them and the microspheres. These patterns can be seen in both the RPMI8226 and U226 cell lines (the behavior of MM1S, was similar to that of the U226 line). It was therefore established that the different microgels allow the growth of myeloma cell lines at least to the same extent as their conventional suspension culture and that most of the microgels respect the suspension growth of the MM cell lines. This result is in itself highly important, as previous research had reported that other commercially available 3D systems (PLGA microspheres, AlgiMatrix, and Matrigel) showed lower MM cell line proliferation rates than conventional 2D cultures [27].

3.3. 3D microgel cultures increased resistance to Bortezomib in vitro

We further evaluated the ability of the different microgels to reproduce resistance to different MM drugs *in vitro*. Dexamethasone (DEX) and bortezomib (BTZ) are currently used for the clinical treatment of MM patients. DEX is a glucocorticoid that induces apoptosis in MM cells through up-regulation of pro-apoptotic genes, down-regulation of anti-apoptotic genes [49], cleavage of poly (ADP-ribose) polymerase and caspase 3 [50] and activation of intrinsic apoptotic pathways [51]. The proteasome inhibitor BTZ is a reversible inhibitor of the 26S proteasome complex. It produces apoptosis in MM cells by different mechanisms such as activation of caspase 8 and 9, upregulation of NOXA [1], or suppression of the NF-KB pathway [52], which is a key regulator of growth and survival in MM cells.

To test the drug efficacy in our 3D model, the cell lines RPMI8226, U226 and MM1.S were grown in all the developed microgels and in suspension without microgels for 72 h in three different conditions: non-treated, DEX 1 μM [25,53] and BTZ 4 nM [54]. In all cases, cell proliferation after 72 h of culture was assessed and the data is represented for each microgel normalized by its non-treated equivalent (Fig. 8).

For the RPMI8226 cell line and the DEX 1 μM treatment, we found that the composition of their polymeric matrix determines the generation of resistance to DEX *in vitro*: the 10% AA microgels have mean proliferation rates which significantly differ from the suspension condition. This means that the presence of acrylic acid increases resistance to DEX *in vitro*. Although there is no significant statistical difference between 10% AA and 10% AA-HA, the HA grafted microgels achieved the higher proliferation rate. This agrees with the reported role of HA as a survival factor against DEX-induced apoptosis in MM cell lines [8]. For cell lines U226 and MM1.S under DEX treatment, microgels did not increase proliferation rate compared to suspension, regardless of the composition or functionalization in either of the two cell lines.

In the case of the BTZ, the microgels yielded very interesting results. Cell line RPMI8226 cultured in suspension had a proliferation rate of 0.04 when treated with BTZ 4 nM. However, when the same cell line was cultured in the different microgels and treated with BTZ 4 nM, the lowest proliferation rate was 0.72, achieved by the 0% AA-FN microgel. The proliferation rates of 0% AA, 10% AA and 10% AA-HA were 0.93, 0.90 and 0.93, respectively. This implies a remarkable increase in cell proliferation with respect to the suspension conditions and shows the ability of the proposed culture systems to generate drug resistance in *in vitro* cultures. Finally, for cell lines U226 and MM1.S, the proliferation rates in suspension when treated with BTZ 4 nM were even lower than 0 (−0.02 and −0.07, respectively) (negative values means cell number after 72 h has decreased to values lower than the 100.000 cells seeded at day 0). When these cells were cultured in the microgels, mean proliferation rates also increase significantly. As in the case of the RPMI8226 cell line, the 0% AA-FN microgel had the lowest proliferation rate followed by the 0% AA microgel. Finally, the 10% AA and 10% AA-HA microgels had the highest proliferation rates with no significant differences. These data reinforce our previous results that pointed to the relevant role of acrylic acid in generating drug resistance in microgel systems. This is even more significant than the functionalization with biomolecules of the BM ECM such as fibronectin or hyaluronic acid.

3.3.1. FN-coated microgels do not generate effective 3D environments

Interestingly, the 0% AA microgel coated with FN had the lowest proliferation for the 3 cell lines treated with BTZ, as well as the RPMI8226 cell line when treated with DEX. It has been reported that FN binding to malignant plasma cells can induce G0/G1 cell cycle arrest and confer drug resistance by means of this mechanism [14,55,56]. To assess whether the reduced MM proliferation in the cell lines cultured in FN-coated microgels was due to G0/G1 arrest, the expression of the Ki67 proliferation marker was quantified by immunofluorescence in RPMI8226 and U226 cell lines cultured in suspension and in the different microgels under non-treated and DEX-treated conditions (Supplementary Fig. 3). Results showed that no significant differences in Ki67 expression were found for RPMI8226 or U226 between the 0% AA and the 0% AA-FN microgels and G0/G1 cell cycle arrest induced by FN could not be confirmed. Supplementary Figs. 4, 5 and 6 show that MM cells distributed homogeneously in all microgels except those FN-coated. In these microgels the 3D distribution was not fully maintained, as the microsphere clusters were heavier. As a result, the FN conditions had a macroscopic distribution similar to that generated by the >70 μm diameter microgels (Fig. 6 d), which stayed at lower proliferation rates than the cell-sized microgels. These differences in the distribution of the microspheres and the formation of groups with cells and by themselves mean that the proliferation data cannot be properly compared with those of other systems. The results shown in Fig. 8 for the FN-coated microgels can be attributed to this phenomenon.

3.3.2. Acrylic acid (AA) contributes to the generation of drug resistance to bortezomib in 3 MM cell lines

Results denote that the presence of AA itself could be a relevant factor for the *in vitro* mimicry of DR. To confirm this result, the viability of the 3 MM cell lines cultured in the 10% AA microgel under non-treated and BTZ-treated conditions was analyzed (Fig. 9). The 10% AA microgel maintained a cell viability of the BTZ treated samples equivalent to their non-treated counterparts.

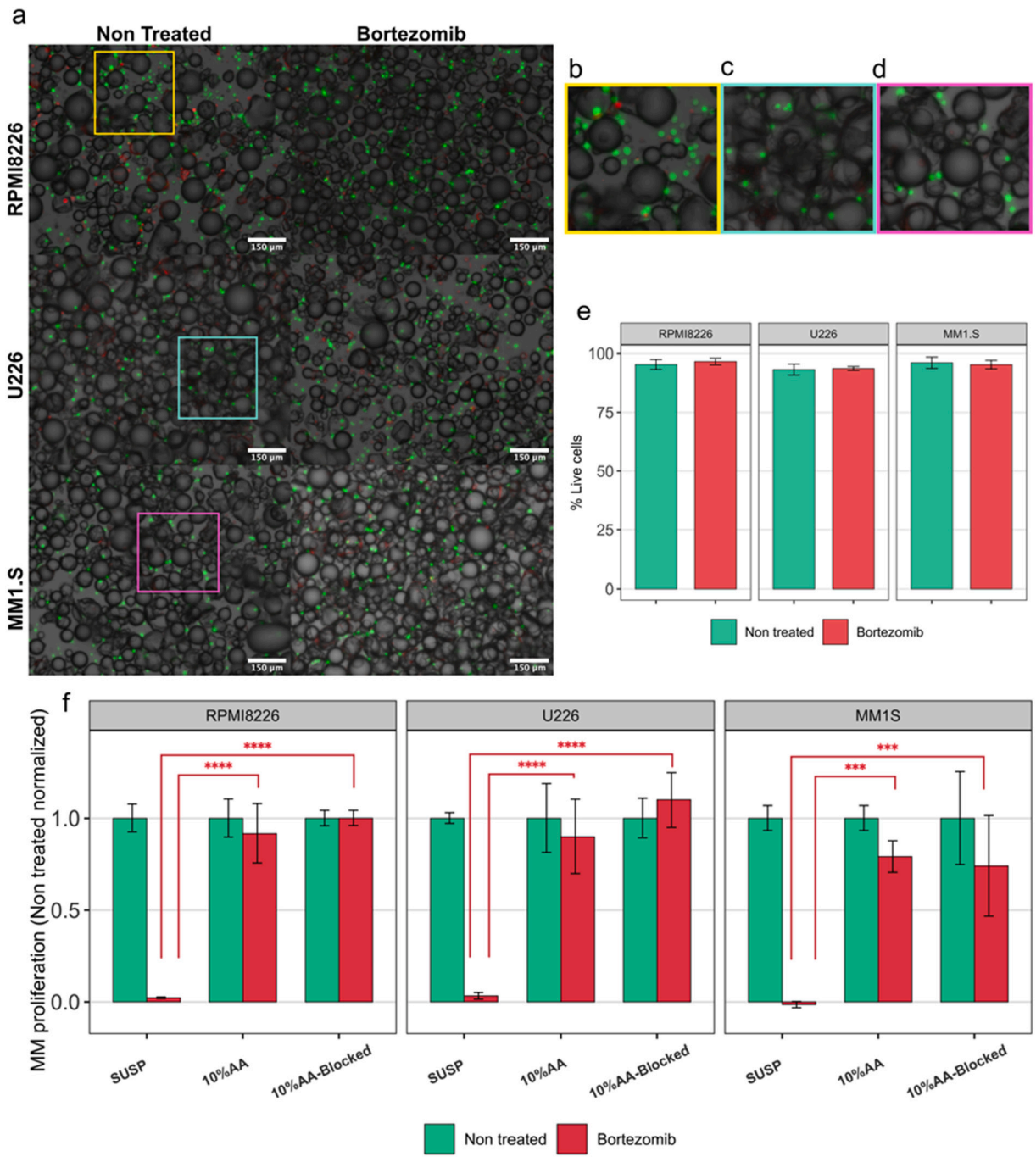

Fig. 9. MM cells treated with BTZ show high viability. a) Images from the Live/Dead staining of the 3 MM cell lines after 72 h of culture in 10% AA microgels under non treated or BTZ 4 nM conditions; green and red represent live and dead cells, respectively (scale bar: 150 µm). b,c,d) Magnified insets of the non-treated images of RPMI8226, U226 and MM1.S from panel a). e) Quantification of viability (mean ± SD, 6 fields from one sample were analyzed). f) Proliferation rates of the cell lines RPMI8226, U226 and MM1.S at 72 h of culture growing in suspension or in microgels when treated with bortezomib 4 nM (red) or non-treated conditions (green). Data is expressed as % of MM proliferation with respect to day 0 and, for each condition, normalized by its non-treated counterpart. SUSP (suspension 2D culture), 10% AA (10% AA ungrafted microgel), 10%AA-Blocked (10% AA with −COOH blocked with ethanolamine). Statistical differences shown in red represent differences between BTZ treated samples. p value legend: $p \leq 0.001$ (***), $p \leq 0.0001$ (****).Comparisons between microgels were made using one-way ANOVA with Tukey's test for post-hoc analysis. (For interpretation of the references to color in this figure legend, the reader is referred to the web version of this article.)

It could be hypothesized that there is a 3D effect that goes further than the specific effect of the biomolecules we studied. However, this theory can be discarded, as the 3D effect could also be expected in the 0% AA microgel. The hypothesis that we put forward is that the acrylic acid present on the surface of the 10%AA microgels enhances their ability to bind and concentrates soluble factors from the medium (either from the FBS or paracrine factors produced by the PCs themselves, such as IL-6) and presents them to the cells more efficiently than the conventional suspension culture, favoring their growth and resistance to drugs. This hypothesis is supported by the fact that the PAA has been reported to have protein-binding properties due to the presence of carboxyl (−COOH) groups, which make their surfaces hydrophilic and improve its adsorption properties [57,58]. In our case, the effects due to AA on microsphere surfaces would be multiplied by the larger specific surface of the microspheres.

To further test this hypothesis 2 different experiments were carried out. First, a 10% AA microgel was coated with bovine serum albumin (BSA), a protein used in research as a competing agent for the unspecific adhesion and generation of non-fouling surface (Supplementary Fig. 7) [59]. Its coating effectiveness and stability were confirmed by XPS and fluorescent labelling after 72 h of culture. Cultures of the RPMI8226 cell line were grown in this microgel under non-treated and DEX treated conditions. The results showed that the BSA antifouling did not significantly affect the proliferation rates of the 10% AA microgel in non-treated conditions or the generation of DEX resistance. Second, a 10% AA microgel with terminal −COOH ethanolamine blocked has been used for the culture of the 3 MM cell lines under non treated and BTZ-treated conditions (Fig. 9, f). The 10%AA-Blocked microgel did not lose the ability of the control microgel to generate resistance to BTZ. This results confirms that the AA effect mechanism is not as simple as increasing cell-microsphere adhesion. Future studies are needed to understand the mechanism underlying the positive effect of AA in terms of generating DR. Several discoveries reported in the literature may lead to the hypothesis that AA interaction with MM cells could condition the cellular phenotype related to the expression of integrins or other surface receptors and thus alter cellular behavior, such as proliferation or DR. In any case, modifying the expression of integrins in the cell could avoid the action of BTZ [60], which needs further studies.

4. Conclusions

We have developed a novel cell culture system based on a semi-solid 3D media defined by microspheres and MM cells growing dynamically in suspension. Microspheres were obtained with different compositions and sizes and effectively functionalized with FN or HA. The effect of microsphere size, composition and functionalization on MM cell lines proliferation was studied. Microgels made of cell-sized microspheres and maintained under 150 rpm stirring supported the proliferation of RPMI8226, U226 and MM1.S MM cell lines. The three MM cell lines cultured in the different microgels showed significantly higher resistance to bortezomib than their conventional 2D cultures. Acrylic acid in the polymeric microsphere matrix showed a positive effect on the generation of resistance to BTZ *in vitro* and will require further studies. The microgel concept introduced here opens the way for novel 3D culture approaches specially designed for cells in suspension. It represents a novel and versatile tool that should be further explored for the 3D culture of hematological malignancies and generation of drug resistance, as it allows biomimetic *in vitro* platforms to be developed that maintain the dynamic and non-adherent properties of lymphoid and myeloid cells.

Data availability statement

The data that support the findings of this study are available from the corresponding author upon reasonable request.

CRediT authorship contribution statement

S. Clara-Trujillo: Conceptualization, Methodology, Validation, Formal Analysis, Investigation, Writing- Original Draft, Visualization. **L. Tolosa**: Methodology, Writing- Review & Editing. **L. Cordón**: Conceptualization, Writing- Review & Editing. **A. Sempere**: Conceptualization, Writing- Review & Editing. **G. Gallego Ferrer**: Conceptualization, Methodology, Formal Analysis, Supervision, Writing- Review & Editing. **J. L. Gómez Ribelles:** Conceptualization, Methodology, Formal Analysis, Supervision, Funding Acquisition, Writing- Review & Editing.

Declaration of competing interest

The authors declare that they have no known competing financial interests or personal relationships that could have appeared to influence the work reported in this paper.

Acknowledgements

This work was funded by the Spanish State Research Agency (AEI) through the PID2019-106099RB-C41/AEI/10.13039/501100011033 Project. CIBER-BBN is an initiative funded by the VI National R&D&I Plan 2008–2011, *Iniciativa Ingenio 2010*, *Consolider* Program. CIBER Actions were financed by the *Instituto de Salud Carlos III* with assistance from the European Regional Development Fund. This work was also supported by the Spanish Ministry of Science, Innovation and Universities through Grant N° FPU17/05810 awarded to Sandra Clara-Trujillo. The Microscopy Service of the UPV (*Universitat Politècnica de València*) is gratefully acknowledged for helping with FESEM characterization.

Appendix A. Supplementary data

Supplementary data to this article can be found online at https://doi.org/10.1016/j.bioadv.2022.212749.

References

[1] V. Pinto, R. Bergantim, H.R. Caires, H. Seca, J.E. Guimaraes, M.H. Vasconcelos, Cancers 12 (2020) 407.
[2] S.V. Rajkumar, Am. J. Hematol. 95 (2020) 548.
[3] R.A. Kyle, M.A. Gertz, T.E. Witzig, J.A. Lust, M.Q. Lacy, A. Dispenzieri, R. Fonseca, S.V. Rajkumar, J.R. Offord, D.R. Larson, M.E. Plevak, T.M. Therneau, P.R. Greipp, Mayo Clin. Proc. 78 (2003) 21.
[4] O. Landgren, B.I. Graubard, J.A. Katzmann, R.A. Kyle, I. Ahmadizadeh, R. Clark, S. K. Kumar, A. Dispenzieri, A.J. Greenberg, T.M. Therneau, L.J. Melton, N. Caporaso, N. Korde, M. Roschewski, R. Costello, G.M. McQuillan, S.V. Rajkumar, Leukemia 28 (2014) 1537.
[5] S.K. Kumar, V. Rajkumar, R.A. Kyle, M. Van Duin, P. Sonneveld, M.V. Mateos, F. Gay, K.C. Anderson, Nat. Rev. Dis. Primers 3 (2017) 17046.
[6] S. Clara-Trujillo, G. Gallego Ferrer, J.L. Gómez Ribelles, Int. J. Mol. Sci. 21 (2020) 5747.
[7] L. Di Marzo, V. Desantis, A.G. Solimando, S. Ruggieri, T. Annese, B. Nico, R. Fumarulo, A. Vacca, M.A. Frassanito, Oncotarget 7 (2016) 60698.
[8] T. Vincent, L. Molina, L. Espert, N. Mechti, Br. J. Haematol. 121 (2003) 259.
[9] B. Katz, Semin. Cancer Biol. 20 (2010) 186.
[10] A. Vacca, M. Di Loreto, D. Ribatti, R. Di Stefano, G. Gadaleta-Caldarola, G. Iodice, D. Caloro, F. Dammacco, Am. J. Hematol. 50 (1995) 9.
[11] T. Okada, R.G. Hawley, M. Kodaka, H. Okuno, Clin. Exp. Metastasis 17 (1999) 623.
[12] G.J. Morgan, B.A. Walker, F.E. Davies, Nat. Rev. Cancer 12 (2012) 335.
[13] H.F. Barker, J. Ball, M. Drew, M.S. Hamilton, I.M. Franklin, Leuk. Lymphoma 8 (1992) 189.
[14] J.S. Damiano, A.E. Cress, L.A. Hazlehurst, A.A. Shtil, W.S. Dalton, Blood 176 (1999) 139.
[15] D. Chauhan, H. Uchiyama, Y. Akbarali, M. Urashima, K.I. Yamamoto, T. A. Libermann, K.C. Anderson, Blood 93 (1996) 1658.
[16] T. Hideshima, P.L. Bergsagel, W.M. Kuehl, K.C. Anderson, Blood 104 (2004) 607.
[17] K. Hatano, J. Kikuchi, M. Takatoku, R. Shimizu, T. Wada, M. Ueda, M. Nobuyoshi, I. Oh, K. Sato, T. Suzuki, K. Ozaki, M. Mori, T. Nagai, K. Muroi, Y. Kano, Y. Furukawa, K. Ozawa, Oncogene 28 (2009) 231.
[18] T. Hideshima, P. Richardson, D. Chauhan, V.J. Palombella, P.J. Elliott, J. Adams, K. C. Anderson, Cancer Res. 61 (2001) 3071.
[19] C.C. Bjorklund, V. Baladandayuthapani, H.Y. Lin, R.J. Jones, I. Kuiatse, H. Wang, J. Yang, J.J. Shah, S.K. Thomas, M. Wang, D.M. Weber, Leukemia 28 (2014) 373.

[20] A. Riedl, M. Schlederer, K. Pudelko, M. Stadler, S. Walter, D. Unterleuthner, C. Unger, N. Kramer, M. Hengstschläger, L. Kenner, D. Pfeiffer, G. Krupitza, H. Dolznig, J. Cell Sci. 130 (2017) 203.
[21] T. Calimeri, E. Battista, F. Conforti, P. Neri, M.T. Di Martino, M. Rossi, U. Foresta, E. Piro, F. Ferrara, A. Amorosi, N. Bahlis, K.C. Anderson, N. Munshi, P. Tagliaferri, F. Causa, P. Tassone, Leukemia 25 (2011) 707.
[22] P. Niemeyer, U. Krause, J. Fellenberg, P. Kasten, A. Seckinger, A.D. Ho, H. G. Simank, Cells Tissues Organs 177 (2004) 68.
[23] P. De La Puente, A.K. Azab, Future Oncol. 12 (2016) 1545.
[24] N.K. Narayanan, B. Duan, J.T. Butcher, A. Mazumder, B.A. Narayanan, In Vivo 28 (2014) 67.
[25] J. Jakubikova, D. Cholujova, T. Hideshima, P. Gronesova, A. Soltysova, T. Harada, J. Joo, S.Y. Kong, R.E. Szalat, P.G. Richardson, N.C. Munshi, D.M. Dorfman, K. C. Anderson, Oncotarget 7 (2016) 47.
[26] R.W.J. Groen, W.A. Noort, R.A. Raymakers, H.J. Prins, L. Aalders, F.M. Hofhuis, P. Moerer, J.F. Van Velzen, A.C. Bloem, B. Van Kessel, H. Rozemuller, E. Van Binsbergen, A. Buijs, H. Yuan, J.D. De Bruijn, M. De Weers, P.W.H.I. Parren, J. J. Schuringa, H.M. Lokhorst, T. Mutis, A.C.M. Martens, Blood 120 (2012) 9.
[27] P. de la Puente, B. Muz, R.C. Gilson, F. Azab, M. Luderer, J. King, S. Achilefu, R. Vij, A.K. Azab, Biomaterials 73 (2015) 70.
[28] S. Poveda-Reyes, V. Moulisova, E. Sanmartín-Masiá, L. Quintanilla-Sierra, M. Salmerón-Sánchez, G. Gallego Ferrer, Macromol. Biosci. 16 (2016) 1311.
[29] L. Pérez-Álvarez, L. Ruiz-Rubio, I. Moreno, J.L. Vilas-Vilela, Polymers 11 (2019) 1843.
[30] C. Mcquin, A. Goodman, V. Chernyshev, L. Kamentsky, A. Cimini, K.W. Karhohs, M. Doan, L. Ding, S.M. Rafelski, D. Thirstrup, W. Wiegraebe, S. Singh, T. Becker, J. C. Caicedo, A.E. Carpenter, PLoS Biol. (2018) 1.
[31] H. Wickham, Elegant Graphics for Data Analysis: ggplot2, Springer-Verlag New York, 2009.
[32] V. Llopis-Hernández, P. Rico, D. Moratal, G. Altankov, M. Salmerón-Sánchez, Bioresearch 2 (2013) 364.
[33] M. Salmerón-Sánchez, P. Rico, D. Moratal, T.T. Lee, J.E. Schwarzbauer, A.J. García, Biomaterials 32 (2011) 2099.
[34] S. Clara-Trujillo, J.C. Marín-Payá, L. Cordón, A. Sempere, G. Gallego Ferrer, J. L. Gómez Ribelles, Colloids Surf. B: Biointerfaces 177 (2019) 68.
[35] E.Y. Liu, S. Jung, H. Yi, Langmuir 32 (2016) 11043.
[36] P.H. Wang, C.Y. Pan, Colloid Polym. Sci. 280 (2002) 152.
[37] S. Poveda-Reyes, T.C. Gamboa-Martínez, S. Manzano, M.H. Doweidar, J.L. Gómez Ribelles, I. Ochoa, G. Gallego Ferrer, Int. J. Polym. Mater. Polym. Biomater. 64 (2015) 745.
[38] G. Gallego Ferrer, M.M. Pradas, J.L.G. Ribelles, P. Pissis, J. Non-Cryst. Solids 235–237 (1998) 692.
[39] P. Robak, I. Drozdz, J. Szemraj, T. Robak, Cancer Treat. Rev. 70 (2018) 199.
[40] W.C. Yang, S.F. Lin, Biomed. Res. Int. 2015 (2015) 341430.
[41] T.M. Tancred, A.R. Belch, T. Reiman, L.M. Pilarski, J. Kirshner, J. Histochem. Cytochem. 57 (2009) 239.
[42] A. Avigdor, P. Goichberg, S. Shivtiel, A. Dar, A. Peled, S. Samira, O. Kollet, R. Hershkoviz, R. Alon, I. Hardan, H. Ben-Hur, D. Naor, A. Nagler, T. Lapidot, Blood 103 (2004) 2981.
[43] S. Trujillo, S.L. Vega, K.H. Song, A. San Félix, M.J. Dalby, J.A. Burdick, M. Salmerón-Sánchez, Adv. Healthc. Mater. 9 (2020) 2000989.
[44] N. Briz, C.M. Antolinos-Turpin, J. Alió, N. Garagorri, J.L.G. Ribelles, J.A. Gómez-Tejedor, J. Biomed. Mater. Res. Part B Appl. Biomater. 101 B (2013) 991.
[45] M. Ferrarini, N. Steimberg, M. Ponzoni, D. Belloni, A. Berenzi, S. Girlanda, F. Caligaris-cappio, G. Mazzoleni, E. Ferrero, PLoS One 8 (2013), e71613.
[46] W. Zhang, W.Y. Lee, D.S. Siegel, P. Tolias, J. Zilberberg, Tissue Eng. Part C Methods 20 (2014) 663.
[47] Q. Jing, H. Cai, Z. Du, Z. Ye, W.S. Tan, Artif. Cells Nanomed. Biotechnol. 41 (2013) 98.
[48] K.S. Carswell, E.T. Papoutsakis, Biotechnol. Bioeng. 68 (2000) 328.
[49] N. Burwick, S. Sharma, Ann. Hematol. 98 (2019) 19.
[50] D. Chauhan, P. Pandey, A. Ogata, G. Teoh, S. Treon, M. Urashima, S. Kharbanda, K. C. Anderson, Oncogene 15 (1997) 837.
[51] D. Chauhan, T. Hideshima, S. Rosen, J.C. Reed, S. Kharbanda, K.C. Anderson, J. Biol. Chem. 276 (2001) 24453.
[52] D. Chen, M. Frezza, S. Schmitt, J. Kanwar, Q.P. Dou, Curr. Cancer Drug Targets 11 (2011) 239.
[53] C. Ohwada, C. Nakaseko, M. Koizumi, M. Takeuchi, S. Ozawa, M. Naito, H. Tanaka, K. Oda, R. Cho, M. Nishimura, Y. Saito, Eur. J. Hematol. 80 (2008) 245.
[54] V. Ramakrishnan, D.E. Mager, J. Pharmacol. Exp. Ther. 365 (2018) 734.
[55] K.H. Shain, D.N. Yarde, M.B. Meads, M. Huang, R. Jove, L.A. Hazlehurst, W. S. Dalton, Cancer Res. 69 (2009) 1009.
[56] L.A. Hazlehurst, J.S. Damiano, I. Buyuksal, W.J. Pledger, W.S. Dalton, Oncogene 19 (2000) 4319.
[57] P.Y. Wang, L.R. Clements, H. Thissend, W.B. Tsaia, N.H. Voelckere, Acta Biomater. 11 (2015) 58.
[58] V. Sharma, K.A. Blackwood, D. Haddow, L. Hook, C. Mason, J.F. Dye, E. García-Gareta, Biochim. Open 1 (2015) 40.
[59] X. Punet, R. Mauchauffé, M.I. Giannotti, J.C. Rodríguez-Cabello, F. Sanz, E. Engel, M.A. Mateos-Timoneda, J.A. Planell, Biomacromolecules 14 (2013) 2690.
[60] S. Sevilla-Movilla, N. Arellano-Sánchez, M. Martínez-Moreno, C. Gajate, A. Sánchez-Vencells, L.V. Valcárcel, X. Agirre, A. Valeri, J. Martínez-López, F. Prósper, F. Mollinedo, J. Teixidó, J. Pathol. 252 (2020) 29.